coatings

MDPI

Article

# Microstructure and Cavitation Erosion Resistance of HVOF Deposited WC-Co Coatings with Different Sized WC

**Xiang Ding [1], Du Ke [2], Chengqing Yuan [2,*], Zhangxiong Ding [2] and Xudong Cheng [1]**

[1] State Key Laboratory of Advanced Technology for Materials and Processing, Wuhan University of Technology, Wuhan 430070, China; dingxiang@whut.edu.cn (X.D.); xudong.cheng@whut.edu.cn (X.C.)
[2] School of Energy and Power Engineering, Wuhan University of Technology, Wuhan 430063, China; kedu_t@whut.edu.cn (D.K.); zxding@whut.edu.cn (Z.D.)
* Correspondence: ycq@whut.edu.cn; Tel.: +86-27-8658-2035

Received: 25 July 2018; Accepted: 24 August 2018; Published: 29 August 2018


**Abstract:** Conventional, multimodal and nanostructured WC-12Co coatings with different WC sizes and distributions were prepared by high velocity oxy-fuel spray (HVOF). The micrographs and structures of the coatings were analyzed by scanning electron microscope (SEM), X-ray diffractometer (XRD) et al. The porosity, microhardness and fracture toughness of the WC-Co coatings were measured. The coating resistance to cavitation erosion (CE) was investigated by ultrasonic vibration cavitation equipment and the cavitation mechanisms were explored. Results show that there is serious WC decarburization in nanostructured and multimodal WC-Co coatings with the formation of $W_2C$ and W phases. The nanostructured WC-Co coating has the densest microstructure with lowest porosity compared to the other two WC-Co coatings, as well as the highest fracture toughness among the three coatings. It was also discovered that the nanostructured WC-Co coating exhibits the best CE resistance and that the CE rate is approximately one-third in comparison with conventional coating.

**Keywords:** WC-12Co coatings; HVOF; microstructure; cavitation erosion

## 1. Introduction

Cavitation erosion (CE) widely exists in the components of fluid equipment, such as marine rudder blades, propellers, and turbine impellers. CE is the predominant cause for overflow part failure and has become one of the most significant technical problems of fluid machinery due to the serious threats to the safety of the machinery, leading to the reduction of the efficiency and the increase of the production cost [1–3]. Therefore, it is of great economic value to improve the CE resistance of the overcurrent components. Since cavitation occurs only in the components' surface, the CE resistance can be improved by surface engineering techniques. Nowadays, various surface engineering techniques, including thermal spraying, laser cladding, physical vapor deposition, chemical vapor deposition, hardening and plasma nitriding, have been developed to enhance the CE resistance of component surfaces. Among them, thermal spraying methods, such as detonation gun, plasma spraying, high velocity oxy-fuel spraying and cold spraying, have already been commercially applied to various machinery components [4–7]. Thermally sprayed WC-Co coatings have attracted much attention in the study of CE resistant coating materials in recent years due to their combination of excellent toughness and high hardness, which is necessary to CE resistance. WC particles and Co binders provide WC-Co coatings with high hardness and excellent toughness, respectively. WC-Co coatings, especially with nano-sized WC particles, have already been successfully utilized in some wear-resistant equipment [8,9].

The mechanical properties and wear performance of WC-Co coatings are largely dependent on WC grain size [10,11]. Recently, simultaneous improvement of the toughness and hardness of nanostructured WC-Co coatings were successfully demonstrated by a number of studies [12–15]. However, the issue of how exactly nano WC affect the wear performance has been a controversial and disputed subject due to various coating fabrication methods and parameters [16,17]. Several researchers have also discovered that the fracture toughness of WC-Co coatings decreases as the WC particle size decreases because of the decarburization of nano WC and the formation of amorphous carbides such as $W_2C$, complex Co-W-C, and metallic W, which can lower the toughness of nanostructured WC-Co coatings [18–20]. The multimodal WC-Co coating composed of nano and micro WC particles, on the other hand, presents lower decarburization and total cost as compared to the nano WC-Co coatings [21–23]. Compared with the conventional WC-Co coatings, multimodal WC coatings offer a denser structure, higher abrasive wear resistance and anti-cavitation performance [24–26]. For example, by comparing the microstructure and surface properties of conventional and nano WC-Co coatings, Zhao et al. [27] concluded lower porosity, higher microhardness and fracture toughness could result from the nano coatings. The microstructure and CE resistance of other multimodal coatings, such as WC-17Co and WC-10Co4Cr have been further investigated by a number of groups [28,29]. However, the relationship of structures, mechanical properties, CE resistance and mechanisms of WC-Co coatings with different WC size have not been studied in details and fully understood.

The coating deposition method is another critical factor influencing the structures and properties of WC-Co cermet coatings. To date, WC-Co coatings are most commonly prepared by HVOF technique because HVOF flame possesses the characteristics of moderate temperature (~2700 °C) and high velocity (600–1200 m/s), which can reduce the decarburization of WC during coating deposition. Therefore, HVOF is thought to be a proper process to deposit WC-Co coatings with nano sized WC particles [30,31].

In the present paper, conventional, multimodal and nanostructured WC-12Co cermet coatings were prepared by HVOF spraying. The structures, mechanical properties and CE performance of the three types of WC-12Co coatings were thoroughly investigated. The CE mechanisms of the coatings were proposed in terms of the formation and propagation of microcracks. These results can provide valuable references for WC-Co anti-cavitation coating design and application.

## 2. Experimental Procedure

### *2.1. Coating Materials*

Nanostructured, conventional and multimodal WC-12Co (88 wt % WC-12 wt % Co) powders were chosen as feedstock in this study and they were marked as NP, CP, and MP, respectively. Both nanostructured WC-12Co powder (S7410, Inframat Advanced Materials LLC, Farmington, CT, USA) and multimodal powder (M1, NEI, Somerset, NJ, USA) were produced by an agglomeration process. The original WC grain size of NP is 50–500 nm, while the volume ratio of micro-sized WC grain (2–3 μm) and nano-sized WC grain (30–50 nm) in MP is 7:3. The size of obtained spraying powder is controlled in the range of 10–45 μm and the mean particle size is 23 μm after agglomeration. On the other hand, the conventional WC-12Co powder (PR4321, Jiorie Thermal Spray Materials Co., Yiyang, China), with a size also between 10 and 45 μm, was fabricated by sintering and crushing process, and the original WC grain size was 2–3 μm.

### *2.2. Coating Fabrication*

The conventional, multimodal and nanostructured WC-12Co coatings were fabricated by a HVOF system (JP5000, Praxair, Inc., Indianapolis, IN, USA) and they were marked as CC, MC and NC, respectively. In the spray system, kerosene and oxygen were used as fuel and oxidant gas. The optimized main spray parameters are shown in Table 1. Due to the variations in particle velocities and temperature characteristics during HVOF spraying for various sized WC-Co materials, deposition

parameters are different for three WC-12Co powders. AISI 304 austenitic stainless steel was chosen as the substrate of coating specimens and as the reference material for comparing the CE resistance of HVOF-sprayed various sized WC-12Co coatings.

**Table 1.** Main spray parameters of WC-12Co coatings by high velocity oxy-fuel spray (HVOF). NP: nanostructured powder; MP: multimodal powder; CP: conventional powder; NC: nanostructured coating; MC: multimodal coating; CC: conventional coating.

| Powder No. | Coating No. | Fuel Flow ($m^3$/h) | Oxygen Flow ($m^3$/h) | Powder Feed Rate (g/min) | Spray Distance (mm) | Horizontal Velocity (mm/s) | Vertical Step (mm) |
|---|---|---|---|---|---|---|---|
| NP | NC | 0.019 | 53.2 | 75 | 370 | 500 | 5 |
| MP | MC | 0.019 | 53.2 | 75 | 370 | 500 | 5 |
| CP | CC | 0.0204 | 61.3 | 75 | 380 | 500 | 5 |

Prior to deposition, the substrates' surface was degreased and grit-blasted with 60 mesh $Al_2O_3$. The coating thickness was in the range of 400 ± 20 μm. All the specimens were machined and polished to surface roughness $R_a \leq 0.02$ μm for coating characterization.

### 2.3. Characterization

An X-ray diffraction system (XRD, D/max-2550 diffraction meter, Rigaku Corporation, Tokyo, Japan) was used for phase identification of the WC-12Co powders and the coatings. The operation of the Cu Kα radiation source was under a voltage of 45 kV and a current of 40 mA. JSM6700F scanning electron microscope (SEM) was carried out to observe the surface morphology and microstructure of the samples. The microhardness of the coatings was measured by a Vickers microhardness tester (Model HV-71, Aolong Xingdi Testing Equipment Co., Shanghai, China). The final value was determined by the average of random ten test points at a loading weight of 200 g and a dwell time of 15 s. The porosity was evaluated by two steps. 500× metallographic photos were first captured by Leitz MM6 metallographic microscope (Leica, Wetzlar, Germany), followed by applying IQ materials software (version 2.0) to calculate porosity. According to [32], fracture toughness can be measured on the transverse section of the coating with a Vickers indenter (HV-5 Vickers hardness tester, 5 kg). Cracks parallel to the substrate surface such as those drawn in Figure 1 would appear on the coating's cross-section. The fracture toughness $K_c$ was calculated according to the Wilshaw Equation (1) and the result was the average value of ten measurements, where $P$, $a$ and $c$ are the load of hardness meter, half the length of indentation diagonal and half the length of the crack, respectively.

$$K_C = 0.079 \frac{P}{a^{3/2}} \log\left(\frac{4.5a}{c}\right) \quad (1)$$

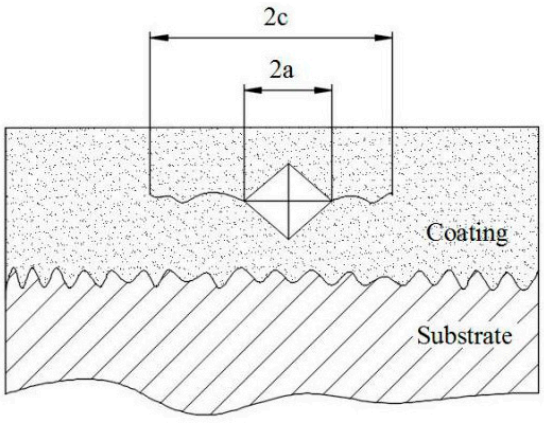


**Figure 1.** Diagram of coating fracture toughness measurement.

### *2.4. Cavitation Erosion Tests*

A J93025 ultrasonic cavitation vibratory equipment was used to evaluate the cavitation erosion of various WC-12Co coatings. The apparatus was set up according to standard GB/T6383-2009 [33], and the schematic diagram is shown in Figure 2. The specimen was machined to the surface roughness $R_a \leq 0.2$ μm before CE tests and then attached to the end of the vibration probe. The samples were weighed every hour by AB204-S electronic balance (Mettler-Toledo GmbH, Greifensee, Switzerland) with the accuracy of 0.1 mg to determine the mass losses during the whole 16-h-test. The volume loss ($\Delta V$) is calculated by mass loss ($\Delta W$) divided by the material density, while the cavitation rate ($R_c$) is calculated by volume loss per hour. In addition, the CE tests of the austenitic stainless steel AISI 304 samples were performed under the same test conditions for comparison.

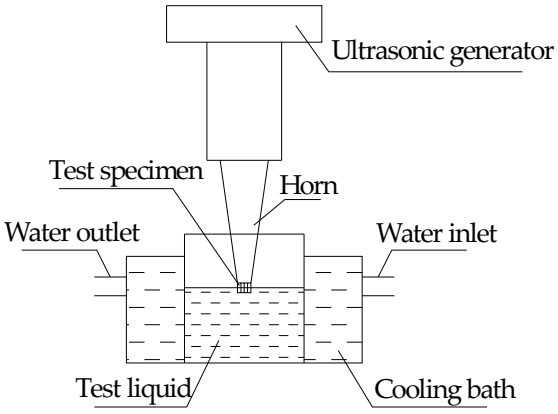


**Figure 2.** Schematic diagram of cavitation erosion (CE) test apparatus.

## 3. Results and Discussion

### *3.1. Microstructure of WC-12Co Powders and Coatings*

The surface micrographs of three WC-12Co powders are present in Figure 3. NP and MP demonstrate spherical shape, but CP shape shows more corners and edges. From CP to MP and NP powder, the WC grains decrease in size meanwhile distribute more evenly. In NP powder, the original crystal WC size is less than 100 nm. The largest grains in CP powder reach 2–3 μm, but a small amount of WC particles remain with a sub-micron size.

The surface morphology of three WC-12Co coatings sprayed by HVOF with different WC sizes are shown in Figure 4. Polygon-shaped, unmolten WC grains can be observed in the CC coating. This suggests that HVOF flame only melts the Co binder, while WC is still in a solid state. In NC and MC coatings, most nano-WC grains are dissolved by heating due to their finer size and higher surface to volume ratio. Among the three WC-Co coatings, NC shows the best melting condition. Thus, the coating microstructures are strongly dependent on the powder structures.

Figure 5 presents the XRD patterns of WC-12Co powders and coatings deposited by HVOF with different WC sizes. The XRD patterns of NP, MP and CP powders show no differences, consisting of pure WC and Co, as shown in the CP pattern. The CC coating has almost identical phase compositions to CP powder, which are mainly composed of WC and Co. For MC and NC coatings, the coatings consist of WC, $W_2C$, and W crystalline phases; the latter two are generated by the decarburization of nano WC. Also, it is demonstrated that an amorphous nanocrystalline zone exists between 35° and 48° at 2θ angles in MC and NC coatings. Although both MP and NP powders suffer typical decarburization during coating deposition, the nanostructured WC-12Co powder had a more serious decarburization rate as more metallic W can be observed in Figure 5. It can be concluded that the decreased size of WC grains is the cause for more serious decarburization, because the larger surface contact area with the flame will give the particles more heat to reach higher temperatures. Figure 6

shows cross-sectional microstructures of three WC-12Co coatings. It can be observed in Figure 6f that the amount of carbides in the NC coating decreased considerably, and more metal phases appeared, which is consistent with the above XRD results.

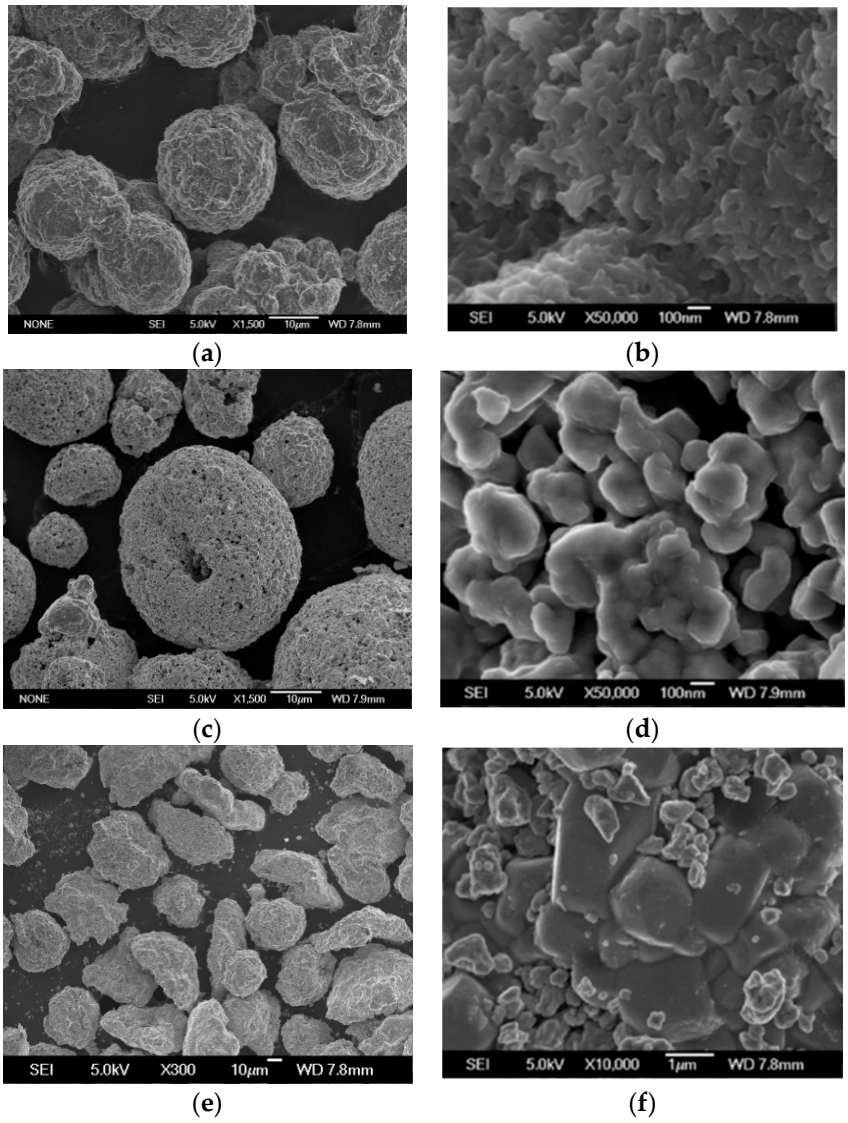


**Figure 3.** SEM micrographs of (**a**,**b**) nanostructured (NP), (**c**,**d**) multimodal (MP), (**e**,**f**) conventional (CP) WC-12Co powders.

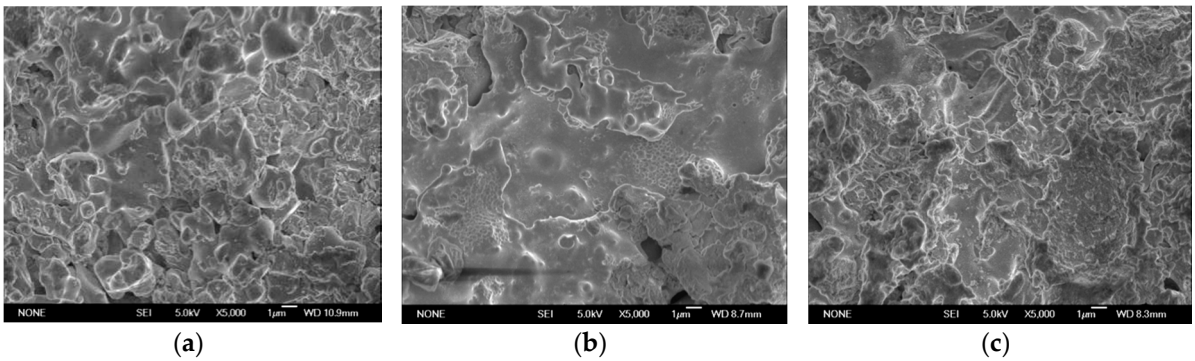


**Figure 4.** Surface micrographs of different structured WC-12Co coatings: (**a**) CC; (**b**) NC; (**c**) MC.

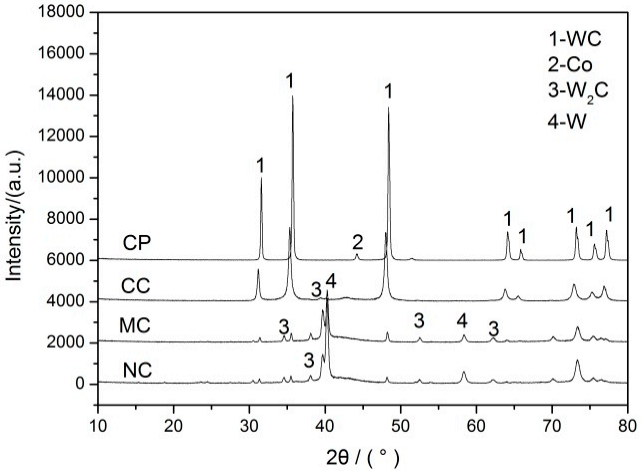


**Figure 5.** XRD patterns of differently structured WC-12Co powders and coatings.

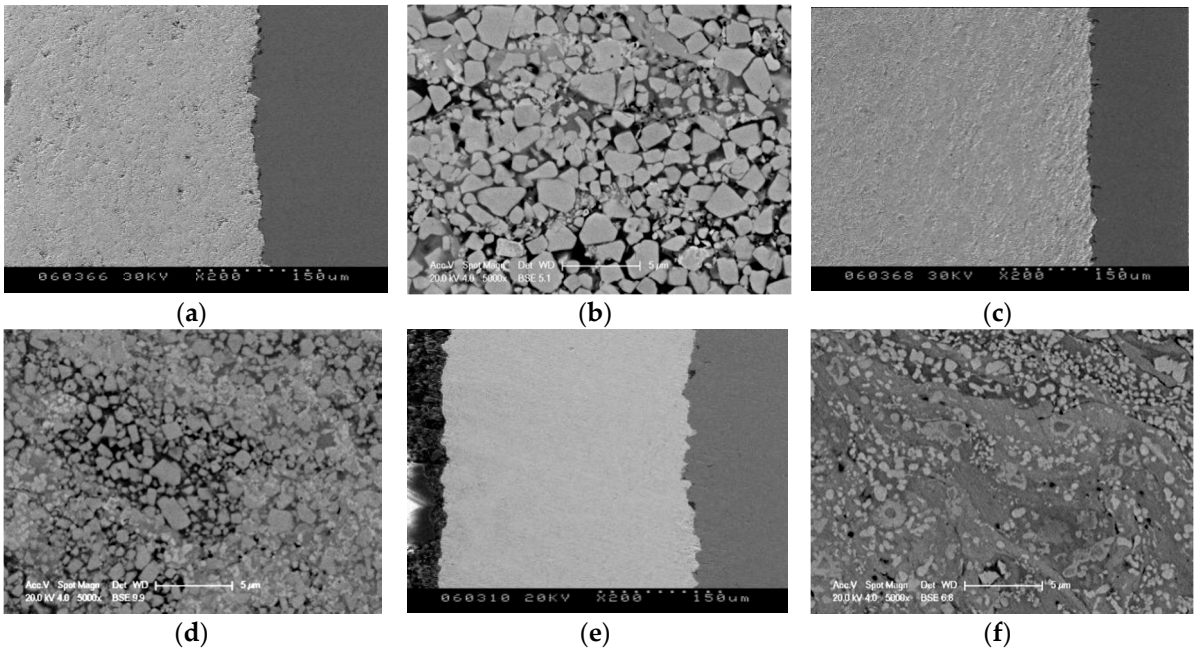


**Figure 6.** Cross-sectional micrographs of different structured WC-12Co coatings: (**a**,**b**) CC; (**c**,**d**) MC; (**e**,**f**) NC.

It can also be observed in Figure 6a,c,e that the microstructures of the three WC-Co coatings are dense and the interlamellar cohesion is strong. The microstructure of NC is densest in comparison with CC and MC coatings. The porosity of CC, MC and NC coatings sprayed by HVOF is shown in Figure 7. It can be seen that NC coating possesses the lowest porosity (0.63% ± 0.11%), at only 36% compared with CC coating (1.76% ± 0.27%). MC coating shows a moderate porosity (1.18 ± 0.21). This indicates that the nanostructured WC-12Co particles possessed more enthalpy and better melting condition before reaching the substrate, given rise to sufficient deformation and growth of denser structure coating.

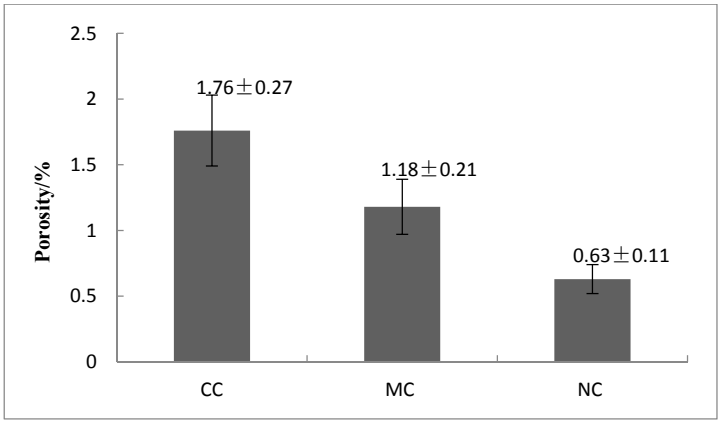


**Figure 7.** Porosity of different structured WC-12Co coatings.

### *3.2. Mechanical Properties of WC-12Co Coatings*

The mechanical properties, including the fracture toughness and microhardness of three different structured WC-Co coatings, are shown in Table 2. The micrographs of fracture toughness indentation of the coatings are presented in Figure 8. It can be seen from Table 2 that the microhardness values of NC and MC coatings are obviously higher than CC coating, as the nano WC particle size decreases and nano WC content increases. The average microhardness values of NC and MC coatings exceed 1500 $HV_{0.2}$ and are 50% higher than the CC coating. It is also observed that the microhardness values of the MC coating change in a larger range than NC coating, although the average microhardness values of NC and MC coatings are almost the same, because WC grain size in MC coating is more disparate, which would influence the coating microhardness variation. Meanwhile, Table 2 demonstrates that the fracture toughness of NC and MC coatings are higher than that of the CC coating, and the highest value is obtained by NC coating. This may be caused by the $W_2C$ and W phase generated during spraying process, in which nano-sized $W_2C$ particles enhance the coating hardness and metallic W phase improves the coating toughness.

**Table 2.** Mechanical properties of different structured WC-12Co coatings.

| Coating No. | Microhardness ($HV_{0.2}$) | Fracture Toughness ($MPa \cdot m^{1/2}$) |
|---|---|---|
| CC | 1034 ± 77.5 | 3.76 ± 0.38 |
| MC | 1523 ± 157.0 | 4.19 ± 0.65 |
| NC | 1541 ± 80.0 | 4.88 ± 0.47 |

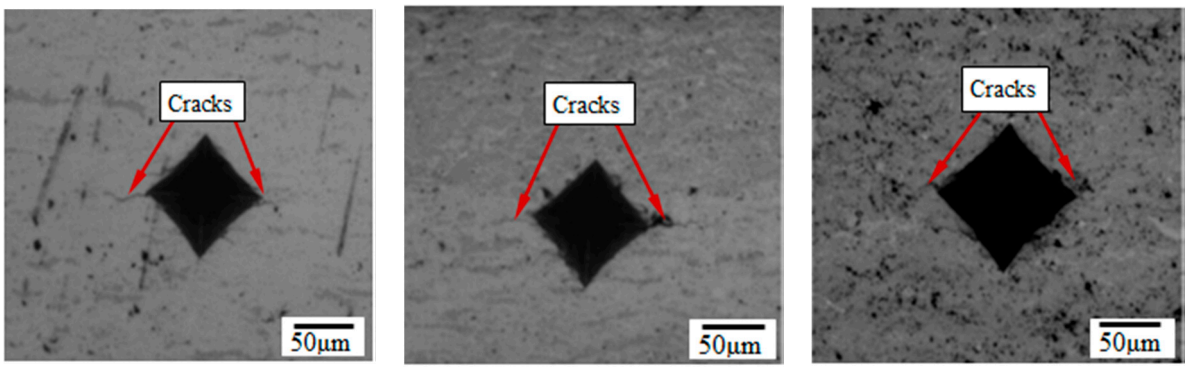


(**a**) (**b**) (**c**)

**Figure 8.** Micrographs of fracture toughness indentation of WC-12Co coatings: (**a**) NC; (**b**) MC; (**c**) CC.

### 3.3. Cavitation Erosion Resistance

The cumulative volume loss curves of 304 stainless steel and three differently structured WC-12Co coatings sprayed by HVOF in fresh water are illustrated in Figure 9. It can be discovered that three WC-Co coatings all possess superior CE resistance than 304 stainless steel after 16 h cavitation, and NC coating displays the best CE resistance increasing more than 60% and 45% more, respectively, than CC and MC coatings.

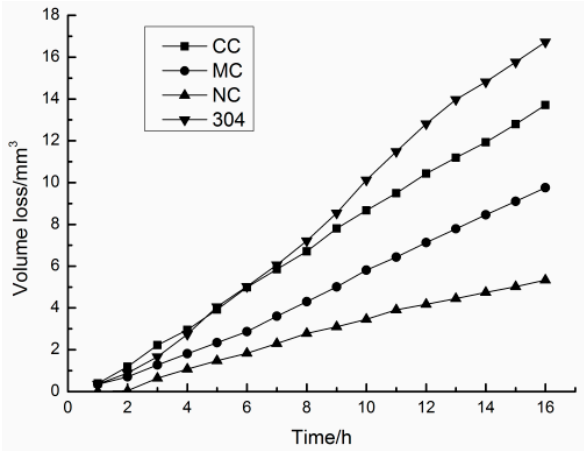


**Figure 9.** Volume loss curves of WC-12Co coatings.

CE rates of 304 stainless steel and three WC-12Co coatings are shown in Figure 10. It can be demonstrated that, in the steady period, the CE rate of CC coating is approximately 1.0 mm$^3$/h, while that of NC coating is 0.3 mm$^3$/h; only 30% of the former. Meanwhile, the CE rate of the MC coating ranks in the middle, at about 70% of the CC coating. It is also seen that in the last testing period (12–16 h), the CE rate of the NC coating displays the tendency to decline compared with the CC coating. From the CE results of Figures 9 and 10, it can be revealed that NC coating with a nano WC size possesses the best CE resistance, while MC coating exhibits moderate CE performance among the three WC-Co coatings.

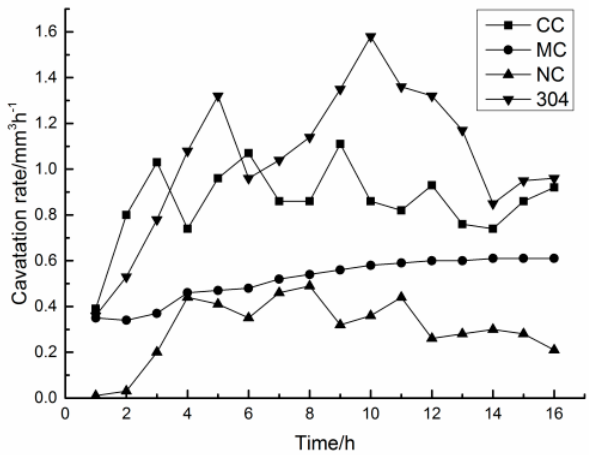


**Figure 10.** Cavitation rates of WC-12Co coatings.

### 3.4. Cavitation Erosion Mechanisms

SEM images of the eroded surfaces of three differently structured WC-12Co coatings after 16 h of CE testing are demonstrated in Figure 11. Due to different CE mechanisms, various eroded surface

micrographs can be observed from different WC-Co coatings. For the CC coating, microcracks initially originate at the weak points on the surface, such as defects, because of the stress concentration under strong alternative stress from the bubble collapsing. The cracks then propagate along the direction of the microjet at the grain boundary, leading to the breakage of brittle phases at the grain boundary and the formation of a cavitation source. In this case, grain can be easily stripped, forming a crater on the coating surface. The growth of craters can further lead coarse WC particles to be removed and lamellar structures to delaminate (Figure 11a).

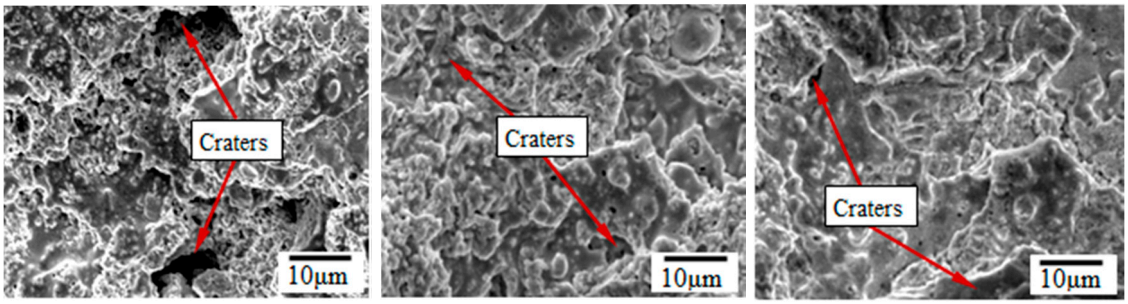


**Figure 11.** Crater micrographs of WC-12Co coatings after 16 h CE: (**a**) CC; (**b**) MC; (**c**) NC.

NC and MC coatings possess a finer and denser microstructure compared to the CC coating since they are composed of nano and sub-micro particles with a sufficient deformation, which diminish the lamellar structure to a certain extent and enhance the cohesive strength between particles. The large area of the particle interface and uniformly distributed grains create a large amount of nanosized grain boundaries, leading to the increase of the coatings' cohesive strength of the grain boundary. Meanwhile, fine particles with superior microhardness such as $W_2C$ can increase the coatings' microhardness. Moreover, the certain amount of W phase with high toughness raises the coatings' fracture toughness. Thus, NC and MC coatings exhibit better CE resistance because the generation and propagation of microcracks are both hindered and only shallow eroded pits can form, as shown in Figure 11b,c. The best CE resistance is realized by the nanostructured WC-12Co coating, which has the highest microhardness and fracture toughness due to the coexistence of nano-sized WC and $W_2C$ particles and tough Co and W metals.

## 4. Conclusions

- WC decarburization occurs during HVOF spraying nanostructured and multimodal WC-12Co powders by forming $W_2C$ and W phases, while no apparent decarburization can be observed using conventional WC-12Co powder. Nanostructured WC-12Co coating suffers the most serious decarburization but possesses the lowest porosity.
- Average microhardness values of nanostructured and multimodal WC-12Co coatings exceed 1500 $HV_{0.2}$, which is 50% higher than the conventional coating. Both coatings also show higher fracture toughness, especially the nanostructured coating.
- Nanostructured and multimodal WC-12Co coatings exhibit the best and intermediate CE resistance, respectively, and the CE rate of nanostructured coating is only approximately one third of that of conventional coating.
- The enhanced CE resistance of the nanostructured WC-12Co coating originates from its superb fracture toughness and microhardness, which makes the microcracks form and propagate with more difficulty. Meanwhile, the coatings dense nanostructure and strong cohesive strength are also factors for the excellent cavitation erosion performance.

**Author Contributions:** Conceptualization, X.D. and Z.D.; Methodology, X.D.; Software, X.D. and D.K.; Validation, X.D., D.K. and C.Y.; Formal Analysis, C.Y.; Investigation, Z.D.; Resources, X.C.; Data Curation, D.K.; Writing—Original Draft Preparation, X.D.; Writing—Review & Editing, X.D. and D.K.; Visualization, Z.D. and X.C.; Supervision, C.Y.; Project Administration, C.Y.; Funding Acquisition, C.Y.

**Funding:** This research was funded by the National Natural Science Foundation of China (No. 51422507).

**Conflicts of Interest:** The authors declare no conflict of interest.

## References

1. Singh, R.; Tiwari, S.K.; Mishra, S.K. Cavitation erosion in hydraulic turbine components and mitigation by coatings: Current status and future needs. *J. Mater. Eng. Perform.* **2012**, *21*, 1539–1551. [CrossRef]
2. Jasionowski, R.; Zasada, D.; Przetakiewicz, W. Cavitation erosion resistance of alloys used in cathodic protection of hulls of ships. *Arch. Metall. Mater.* **2014**, *59*, 241–245. [CrossRef]
3. Kim, J.H.; Yang, H.S.; Baik, K.H.; Seong, B.G.; Lee, C.H.; Hwang, S.Y. Development and properties of nanostructured thermal spray coatings. *Curr. Appl. Phys.* **2006**, *6*, 1002–1006. [CrossRef]
4. Kamdi, Z.; Shipway, P.H.; Voisey, K.T.; Sturgeon, A.J. Abrasive wear behavior of conventional and large-particle tungsten carbide-based cermet coatings as a function of abrasive size and type. *Wear* **2011**, *271*, 1264–1272. [CrossRef]
5. Tillmann, W.; Baumann, I.; Hollingsworth, P.S.; Hagen, L. Sliding and rolling wear behavior of HVOF-sprayed coatings derived from conventional, fine and nanostructured WC-12Co powders. *J. Therm. Spray Technol.* **2014**, *23*, 262–280. [CrossRef]
6. Krebs, S.; Grtner, F.; Klassen, T. Cold spraying of Cu-Al-Bronze for cavitation protection in marine environments. *J. Therm. Spray Technol.* **2015**, *45*, 708–716.
7. Wang, Y.; Liu, J.; Kang, N.; Darut, G.; Poirier, T.; Stella, J.; Liao, H.; Planche, M.H. Cavitation erosion of plasma-sprayed CoMoCrSi coatings. *Tribol. Int.* **2016**, *102*, 429–435. [CrossRef]
8. Ma, N.; Guo, L.; Cheng, Z.; Wu, H.; Ye, F.; Zhang, K. Improvement on mechanical properties and wear resistance of HVOF sprayed WC-12Co coatings by optimizing feedstock structure. *Appl. Surf. Sci.* **2014**, *320*, 364–371. [CrossRef]
9. Guilemany, J.M.; Dosta, S.; Miguel, J.R. The enhancement of the properties of WC-Co HVOF coatings through the use of nanostructured and microstructured feedstock powders. *Surf. Coat. Technol.* **2006**, *201*, 1180–1190. [CrossRef]
10. Lekatou, A.; Sioulas, D.; Karantzalis, A.E.; Grimanelis, D. A comparative study on the microstructure and surface property evaluation of coatings produced from nanostructured and conventional WC-Co powders HVOF-sprayed on Al7075. *Surf. Coat. Technol.* **2015**, *276*, 539–556. [CrossRef]
11. Babua, P.S.; Basub, B.; Sundararajan, G. Abrasive wear behavior of detonation sprayed WC-12Co coatings: Influence of decarburization and abrasive characteristics. *Wear* **2010**, *268*, 1387–1399. [CrossRef]
12. Cho, T.Y.; Yoon, J.H.; Kim, K.S.; Song, K.O.; Joo, Y.K.; Fang, W.; Zhang, S.H.; Youn, S.J.; Chun, H.G.; Hwang, S.Y. A study on HVOF coatings of micron and nano WC-Co powders. *Surf. Coat. Technol.* **2008**, *202*, 5556–5559. [CrossRef]
13. Yang, Q.; Senda, T.; Ohmori, A. Effect of carbide grain size on microstructure and sliding wear behavior of HVOF-sprayed WC-12%Co coatings. *Wear* **2003**, *254*, 23–34. [CrossRef]
14. He, J.; Lavernia, E.J.; Liu, Y.; Qiao, Y.; Fischer, T.E. Near-nanostructured WC-18 pct Co coatings with low amounts of non-WC carbide phase: Part I. synthesis and characterization. *Metall. Mater. Trans. A* **2002**, *33*, 145–157. [CrossRef]
15. Ji, G.C.; Wang, H.T.; Chen, X.; Bai, X.B.; Dong, Z.X.; Yang, F.G. Characterization of cold-sprayed multimodal WC-12Co coating. *Surf. Coat. Technol.* **2013**, *235*, 536–543. [CrossRef]
16. Wang, Q.; Chen, Z.H.; Li, L.X.; Yang, G.B. The parameters optimization and abrasion wear mechanism of liquid fuel HVOF sprayed bimodal WC-12Co coating. *Surf. Coat. Technol.* **2012**, *206*, 2233–2241. [CrossRef]
17. Ding, Z.X.; Chen, W.; Wang, Q. Resistance of cavitation erosion of multimodal WC-12Co coatings sprayed by HVOF. *Trans. Nonferrous Met. Soc. China* **2011**, *21*, 2231–2236. [CrossRef]
18. Ding, X.; Cheng, X.D.; Shi, J.; Li, C.; Yuan, C.Q.; Ding, Z.X. Influence of WC size and HVOF process on erosion wear performance of WC-10Co4Cr coatings. *Int. J. Adv. Manuf. Technol.* **2018**, *96*, 1615–1624. [CrossRef]

19. Hu, Y.M. Structure and Resistance of Cavitation Erosion Micro-Nano WC-Based Coatings Sprayed by HVOF. Master's Thesis, Wuhan University of Technology, Wuhan, Hubei, China, 2015. (In Chinese)
20. Ghabchi, A.; Varis, T.; Turunen, E.; Suhonen, T.; Liu, X.; Hannula, S.P. Behavior of HVOF WC-10Co4Cr coatings with different carbide size in fine and coarse particle abrasion. *J. Therm. Spray Technol.* **2010**, *19*, 368–377. [CrossRef]
21. Wang, H.T.; Ji, G.C.; Chen, Q.Y.; Du, X.F.; Fu, W. Microstructure characterization and abrasive wear performance of HVOF sprayed WC-Co coatings. *Adv. Mater. Res.* **2011**, *189–193*, 707–710. [CrossRef]
22. Hong, S.; Wu, Y.P.; Zhang, J.F.; Zheng, Y.G.; Zheng, Y.; Lin, J.R. Synergistic effect of ultrasonic cavitation erosion and corrosion of WC-CoCr and FeCrSiBMn coatings prepared by HVOF spraying. *Ultrason. Sonochem.* **2016**, *31*, 563–569. [CrossRef] [PubMed]
23. Wang, Q.; Tang, Z.X.; Cha, L.M. Cavitation and sand slurry erosion resistances of WC-10Co-4Cr coatings. *J. Mater. Eng. Perform.* **2015**, *24*, 2435–2443. [CrossRef]
24. Rodríguez, M.A.; Gil, L.; Camero, S.; Fréty, N.; Santana, Y.; Caro, J. Effects of the dispersion time on the microstructure and wear resistance of WC/Co-CNTs HVOF sprayed coatings. *Surf. Coat. Technol.* **2014**, *258*, 38–48. [CrossRef]
25. Ding, X.; Cheng, X.D.; Li, C.; Yu, X.; Ding, Z.X.; Yuan, C.Q. Microstructure and performance of multi-dimensional WC-CoCr coating sprayed by HVOF. *Int. J. Adv. Manuf. Technol.* **2018**, *96*, 1625–1633. [CrossRef]
26. Hong, S.; Wu, Y.P.; Zhang, J.F.; Zheng, Y.G.; Qin, Y.J.; Gao, W.W.; Li, G.Y. Cavitation erosion behavior and mechanism of HVOF sprayed WC-10Co-4Cr coating in 3.5 wt.% NaCl solution. *Trans. Indian Inst. Met.* **2015**, *68*, 151–159. [CrossRef]
27. Zhao, X.Q.; Zhou, H.D.; Chen, J.M. Comparative study of the friction and wear behavior of plasma sprayed conventional and nanostructured WC-12%Co coatings on stainless steel. *Mater. Sci. Eng. A* **2006**, *431*, 290–297. [CrossRef]
28. Wang, H.T.; Chen, X.; Bai, X.B.; Ji, G.C.; Dong, Z.X.; Yi, D.L. Microstructure and properties of cold sprayed multimodal WC-17Co deposits. *Int. J. Refract. Met. Hard Mater.* **2014**, *45*, 196–203. [CrossRef]
29. Ding, X.; Cheng, X.D.; Yuan, C.Q.; Shi, J.; Ding, Z.X. Structure of micro-nano WC-10Co4Cr coating and cavitation erosion resistance in NaCl solution. *Chin. J. Mech. Eng. Engl. Ed.* **2017**, *30*, 1239–1247. [CrossRef]
30. Ding, X.; Cheng, X.D.; Yu, X.; Li, C.; Yuan, C.Q.; Ding, Z.X. Structure and cavitation erosion behavior of HVOF sprayed multi-dimensional WC-10Co4Cr coating. *Trans. Nonferrous Met. Soc. China* **2018**, *28*, 487–494. [CrossRef]
31. Al-Mutairi, S.; Hashmi, M.S.J.; Yilbas, B.S.; Stokes, J. Microstructural characterization of HVOF/plasma thermal spray of micro/nano WC-12%Co powders. *Surf. Coat. Technol.* **2015**, *264*, 175–186. [CrossRef]
32. Sahraoui, T.; Guessasma, S.; Jeridane, M.L.; Hadji, M. HVOF sprayed WC-Co coatings: Microstructure, mechanical properties and friction moment prediction. *Mater. Des.* **2010**, *31*, 1431–1437. [CrossRef]
33. *GB/T 6383-2009 The Method of Vibration Cavitation Erosion Test*; Standards Administration of China: Beijing, China, 2009.